

# Compound events of heatwave and dust storm in the Taklamakan Desert

Yuzhi LIU<sup>1,2†</sup>, Jianping HUANG<sup>1,2\*</sup>, Ziyuan TAN<sup>1†</sup>, Chenglong ZHOU<sup>1,3</sup>, Dan LI<sup>1</sup> & Yongkun XIE<sup>2</sup>

<sup>1</sup> Key Laboratory for Semi-Arid Climate Change of the Ministry of Education, Lanzhou University, Lanzhou 730000, China;

<sup>2</sup> Collaborative Innovation Center for Western Ecological Safety, Lanzhou University, Lanzhou 730000, China;

<sup>3</sup> Taklamakan National Station of Observation and Research for Desert Meteorology in Xinjiang, Urumqi 830002, China

Received November 21, 2023; revised May 28, 2024; accepted May 30, 2024; published online June 14, 2024

**Abstract** Taklamakan Desert (TD) has been characterized by numerous heatwaves and dust storms, leading to negative effects on societies and ecosystems at regional and global scales. However, the association between heatwaves and dust storms is poorly known. In this study, we describe the association between heatwaves and dust events and propose a mechanism for such compound events in the TD. The results show that, from 1993 to 2022, the frequency and intensity of heatwaves in the TD have increased at a rate of  $0.21 \text{ days year}^{-1}$  and  $0.02^\circ\text{C year}^{-1}$ , respectively. More than 40% of heatwaves existed with dust events, which significantly lagged behind heatwaves. Mechanically, the higher the air temperature, the hotter and drier the soil, leading to more dust emissions in the TD. In high-occurrence heatwave years, a large-scale wave train of “cyclone-anticyclone-cyclone” in the northwest-southeast direction was found, with the anticyclone of which hovered over the TD region. The anomalous anticyclones favored the formation and maintenance of heatwaves, and subsequent anomalous cyclones in the wave train triggered strong dust events followed by heatwaves. With climate warming, the compound events of heatwave and dust storm are becoming bigger hazards threatening the socioeconomic and ecological security in the TD, the profound study of which is critical to understanding regional extreme responses.

**Keywords** Heatwave, Dust storm, Compound events, Taklamakan Desert

**Citation:** Liu Y, Huang J, Tan Z, Zhou C, Li D, Xie Y. 2024. Compound events of heatwave and dust storm in the Taklamakan Desert. *Science China Earth Sciences*, 67, <https://doi.org/10.1007/s11430-023-1355-1>

## 1. Introduction

Since the late 19th century (IPCC, 2013, 2021), annual and seasonal means of near-surface air temperature have increased in numerous regions worldwide. According to the World Meteorological Organization, a heatwave event occurs when the maximum daily temperature exceeds  $32^\circ\text{C}$  for more than 3 days (Smoyer-Tomic et al., 2003). Heatwaves pose disastrous impacts on human society and ecosystems, including excess mortality in the population (Robine et al.,

2008) and reduce vegetation productivity (Bastos et al., 2014). Moreover, they are often linked to rapidly emerging flash droughts (Yuan et al., 2019). Therefore, examining the behaviors and impacts of heatwaves is critical.

Compared with humid regions, arid regions suffer severely from frequent and severe heatwaves. The Taklamakan Desert (TD), located in the Tarim Basin of the Xinjiang Autonomous Region of China, is considered the driest area of the Asian mid-latitude arid zone and one of the major sources of global dust (Wang et al., 2005; Zhou et al., 2022a, 2022b). Serious heatwaves reportedly occur frequently in the TD, especially dry heatwave events (Ding et al., 2010), whereas

\* Corresponding author (email: [hip@lzu.edu.cn](mailto:hip@lzu.edu.cn))

† The authors contributed equally to this work

heatwave-drought compound events tend to have more severe consequences (Feng et al., 2019).

Influenced by global warming, monsoons, and sea surface temperature anomalies (Wu and Yu, 2016; Jin et al., 2018), the frequency, intensity, duration, and extent of global heatwave-drought compound events tend to increase (Wu et al., 2021), especially in drylands such as the TD, where the increase rates are almost twice as much as those in humid regions (Wang et al., 2023). Further, drought causes more dust emission (Aryal and Evans, 2021), which in turn produces stronger drought-dust storm compound events (Pu et al., 2022), causing significant increases in dust storms under drought conditions since the 1990s (Zou et al., 2005). Moreover, some previous studies revealed there are relationships between dust events and heatwaves. For example, Wang et al. (2009) reported a significant positive correlation between the daily range of air temperature and days with dust storms in Inner Mongolia of China. The results of Lyamani et al. (2006) also showed that during a heatwave episode in southeastern Spain, the fine particle concentration was higher than that obtained after the heatwave. To comprehensively understand the features and evolution of dust activity, in-depth investigations of heatwaves in the TD are warranted.

Previous studies demonstrated that heatwaves respond sensitively to global climate change in the TD because of its extremely dry climate (Qian et al., 2001). Some researchers reported that in the Xinjiang Autonomous Region of China, the air temperature increased at a rate of 0.33–0.36°C per decade from 1960 to 2010 (Li et al., 2013). Furthermore, the frequency of extreme high-temperature days exhibited a significant increasing trend during 1950–2009 at a rate of 1.8 days per decade (Chen et al., 2012). Therefore, investigations into how dust events respond to heatwaves in the TD are critical to broadening the scientific understanding of the dust activity responses in the TD region to global warming.

## 2. Data and methodology

### 2.1 Ground-based measurements

In this study, ground-based observations, including daily maximum air temperature (DMAT) and weather phenomenon, derived from 27 meteorological stations in the summer from 1993 to 2022 are used. These 27 meteorological stations are affiliated with the national stations of China, which are distributed around and within the TD. The details of the station locations and altitudes are listed in Table 1. The temporal resolutions of the DMAT and weather phenomenon data is 1 day.

For the case analysis, ground-based hourly observations of particulate matter (PM) concentrations from four environmental monitor stations are used: Kuerle (KEL, located in

the eastern TD), Kashi (KS, located in the western TD), Hetian (HT, located in the southern TD), and Akesu (AKS, located in the northern TD).

### 2.2 Satellite observations

The Moderate-Resolution Imaging Spectroradiometer (MODIS) onboard the Terra and Aqua satellites can provide global aerosol data with high spatial resolution near day-to-day (Kaufman et al., 1997; Sayer et al., 2013). In this study, we utilized aerosol optical depth (AOD) at 550 nm from MOD08\_D3 (daily,  $1.0^\circ \times 1.0^\circ$ ) and MOD08\_M3 products (monthly,  $1.0^\circ \times 1.0^\circ$ ) to analyze the characteristics of aerosol extinction.

### 2.3 Reanalysis data

ERA5, the latest atmospheric reanalysis product produced by the European Centre for Medium-Range Weather Forecasts, provides hourly data for various atmospheric, land-surface, and sea-state parameters. Herein, 2-m temperature of the single level from ERA5 (Hersbach et al., 2020) were used to analyze the characteristics of heatwaves ( $0.25^\circ \times 0.25^\circ$ , hourly, 2000–2022). The temperature,  $u$ - and  $v$ -components of wind, vertical velocity, specific humidity, and geopotential on the pressure levels (1000–100 hPa,  $0.25^\circ \times 0.25^\circ$ , monthly, 2000–2022) from ERA5 were used to investigate the atmospheric circulation anomalies of the compound events.

Global Land Data Assimilation System (GLDAS) was jointly developed by the National Aeronautics and Space Administration, the National Centers for Environmental Prediction, and the National Oceanic and Atmospheric Administration (Rodell et al., 2004). In this study, soil temperatures at 0–10 cm underground and soil moisture at 0–10 cm underground ( $0.25^\circ \times 0.25^\circ$ , monthly and daily, 2000–2022) from NOAH0.25\_v2.1 were used to investigate the soil temperature and moisture of the superficial ground layer because of their better performance in the TD (Bai et al., 2018; Yang and Zhang, 2018), which was associated with dust emission.

### 2.4 Definition of heatwaves, dust events, and compound events

In this study, we adopted the definition of heatwave provided by the China Meteorological Administration, considering daily maximum temperatures equal to or greater than 35°C for more than three consecutive days. This definition is tailored to the geographical location and climate of China and is more consistent with general perception and body feelings. Besides, in the analysis of dust events, a day is defined as a “dust day” when a dust storm, flowing dust, or blowing dust occurs at any time of the day based on manually reported

**Table 1** Locations and altitudes of 27 stations in the TD

Station	Altitude (m)	Latitude /longitude (°)	Station	Altitude (m)	Latitude /longitude (°)	Station	Altitude (m)	Latitude /longitude (°)
Akesu (AKS)	1103.8	41.17/ 80.23	Keping (KP)	1161.8	40.50/ 79.05	Tazhong (TZ)	1099.3	39.00/ 83.67
Alaer (ALE)	1012.2	40.55/ 81.27	Luopu (LP)	1347.9	37.08/ 80.17	Tiganlike (TGLK)	846	40.63/ 87.70
Atushi (ATS)	1298.7	39.72/ 76.17	Maigaiti (MGT)	1178.2	38.92/ 77.63	Wushi (WS)	1395.8	41.22/ 79.23
Awati (AWT)	1044.3	40.65/ 80.40	Minfeng (MF)	1409.5	37.07/ 82.72	Xinhe (XH)	1009.8	41.55/ 82.65
Cele (CL)	1336.5	37.02/ 80.80	Moyu (MY)	1348.9	37.17/ 79.63	Yecheng (YC)	1360.4	37.92/ 77.40
Jiashi (JS)	1208.6	39.50/ 76.73	Pishan (PS)	1375.4	37.62/ 78.28	Yingjisha (YJS)	1297.5	38.93/ 76.17
Hetian (HT)	1375	37.13/ 79.93	Qiemu (QM)	1247.2	38.15/ 85.55	Yutian (YT)	1422	36.85/ 81.65
Kashi (KS)	1385.6	39.48/ 75.75	Shaya (SY)	980.4	41.23/ 82.78	Yuepuhu (YPH)	1206.3	39.25/ 76.78
Kerle (KEL)	931.5	41.75/ 86.13	Shache (SC)	1231.2	38.43/ 77.27	Zepu (ZP)	1274.7	38.20/ 77.27

weather information. Heatwave-dust compound events are defined as those characterized by the presence of both heatwaves and dust events.

### 3. Results and analyses

#### 3.1 Feature of heatwaves in the TD region

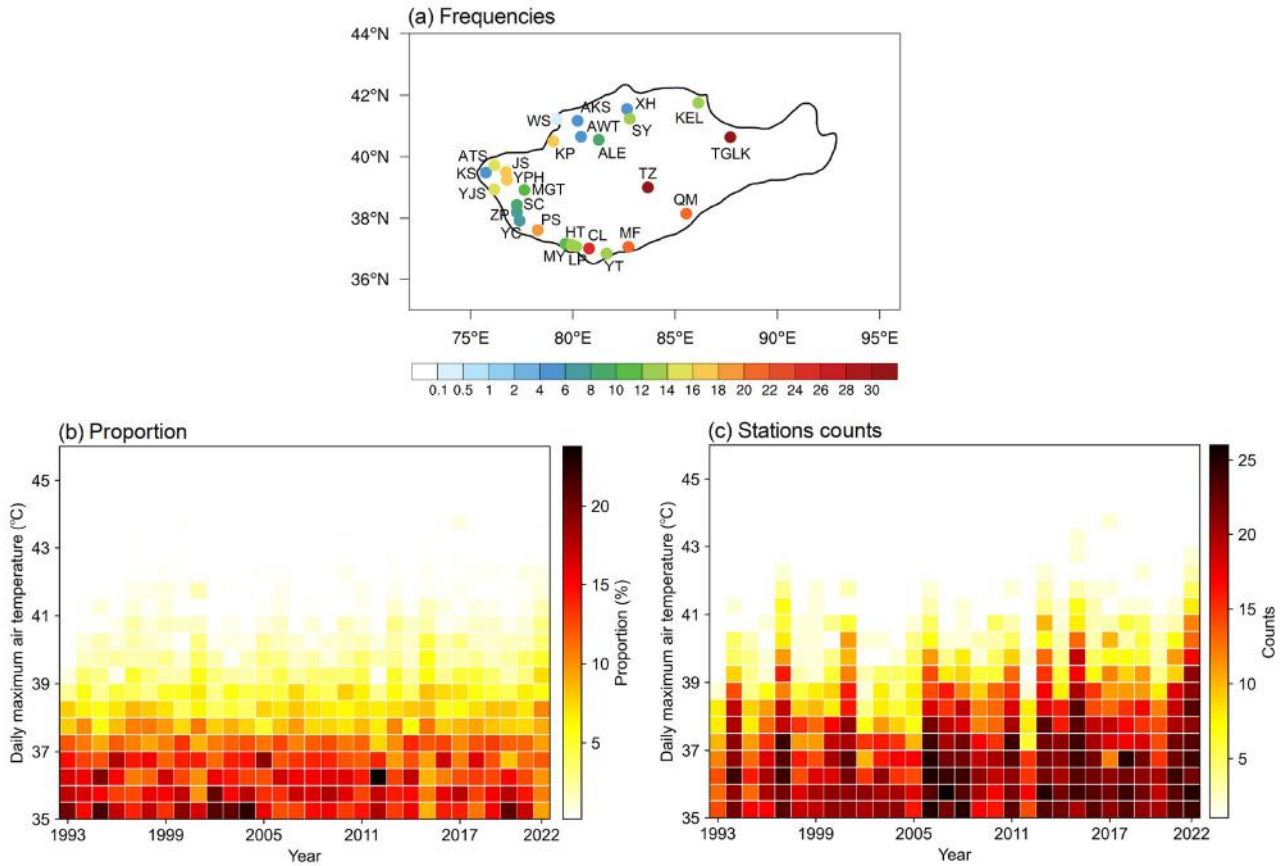
Figure 1 shows the distribution and time series of heatwave frequency in the TD during 1993–2022. As shown in Figure 1a, heatwaves severely hit the TD in summer during the past 30 years (1993–2022). Overall, the southern TD experienced more frequent heatwaves compared with the northern region, with the maximum frequencies (over 30 days per year) in the central TD. In view of the time series of heatwave frequencies, as given in Figure 1b, during most heatwave days, DMAT ranged from 35°C to 37.5°C during 1993–2022. Since 2001, more heatwaves with DMAT over 38°C have occurred, and more portions of heatwaves with DMAT over 39°C were observed in 2022. Heatwaves with DMAT over 41°C showed an increasing trend from 1993 to 2022. Besides, the stations hit by heatwaves with different intensities were counted, as indicated in Figure 1c. Over the last 30 years, stronger heatwaves have been increasingly observed at more stations. Meanwhile, a quasiperiodic oscillation phenomenon in heavy heatwaves with DMAT exceeding 39°C is shown in Figure 1c.

Figure 2 shows the trend distribution of heatwave frequencies and DMAT during 1993–2022 in the TD. In Figure 2a, all stations except for four (KEL, TZ, PS, and MY) ex-

perienced an increase in the frequency of heatwaves at a rate of 0.21 days year<sup>-1</sup> during the past 30 years. The maximum increase (0.60 days year<sup>-1</sup>) in heatwave frequencies was found in the western TD, including the JS, YPH, and MGT stations. Figure 2b shows the trend distribution of DMAT. As indicated in Figure 2b, most stations (except for AKS, ATS, SC, PS, and MY) were hit by intensified heatwaves with a DMAT increase rate of 0.02°C year<sup>-1</sup>. Notably, although the heatwaves at the TZ station (located in the center of the TD) showed a decreasing trend, the intensity of heatwaves (reflected by DMAT) showed enhancement. For the SC station, the DMAT showed a decreasing trend, but the frequency of heatwaves showed a growth tendency. Therefore, combining the changes in heatwave frequencies and intensities as given in Figure 2, the heatwaves showed an increasing tendency during the past 30 years in the TD.

#### 3.2 Dust events associated with heatwaves

To better understand the potential influence of heatwaves on dust events, a compound process of dust event and heatwave (hereinafter referred to as heatwave-dust) that occurred from June 25 to July 13, 2022, was analyzed in detail. Figure 3 shows the DMAT anomalies and DMAT/PM time series from June 25 to July 13, 2022, in the TD. As shown in Figure 3a, DMAT during this typical process was 3–7°C higher relative to the 30-year average (1993–2022). Here, we selected four stations located in the east (KEL), west (KS), south (HT), and north (AKS) of the TD to analyze the details of the heatwave-dust process in different regions, as given in Fig-



**Figure 1** (a) Frequency distribution of heatwaves (day), (b) time series of the proportion (%) of heatwaves with different intensities at all sites in the TD region, and (c) number of stations where heatwaves occurred with different intensities in summer from 1993 to 2022. The dots in (a) indicate the site locations (details are listed in Table 1), whereas the shadings indicate different frequencies. The region enclosed by the solid curve indicates the Tarim Basin where the TD is located.

ures 3b–3e. Overall,  $PM_{2.5}$  (diameter  $\leq 2.5 \mu m$ ) and  $PM_{10}$  (diameter  $\leq 10 \mu m$ ) concentrations were relatively lower during the heatwave process. Then, they began to sharply increase when heatwaves weakened to disappeared, implying a certain lag between dust event and heatwave in the TD. Figure 3f shows the mean DMAT/PM time series at four typical stations during the typical heatwave-dust process, which clearly indicates the above lagging phenomenon. This is because thermodynamics plays a crucial role in the occurrence of dust weather, which involves a process of energy accumulation and release (Zhou et al., 2019).

Furthermore, the spatial distributions of 2-m air temperature and AOD in the TD during the heatwave-dust event from July 2 to 10 were analyzed, as presented in Figure 4. On July 2, the air temperature in the whole TD reached  $35^{\circ}C$  or even higher, implying the beginning of a heatwave. As the heatwave developed, the air temperature in the TD gradually increased. On July 4, the air temperature in the southern TD exceeded  $40^{\circ}C$ , and the heatwave developed to the strongest stage on July 5, with the air temperature in almost the whole TD reaching over  $40^{\circ}C$ . Then, on July 6, accompanied by the weakened heatwave, a dust storm began, with temperatures

over  $35^{\circ}C$  throughout the TD except in the southwest part, where the air temperature still exceeded  $40^{\circ}C$  and where there was no dust storm. Simultaneously, dust emission began in the central and eastern TD, and some areas with high values of AOD over 1.5 appeared. With the strengthening of the dust emission on July 7, the dust concentration increased significantly in the TD, and the AOD exceeded 2.0 in the whole TD except for the northwestern area. Then, the heatwave further weakened, and the air temperature in the central and eastern TD remained between  $35^{\circ}C$  and  $40^{\circ}C$ , whereas it decreased to below  $35^{\circ}C$  in the western TD. On July 8, the dust event developed southwestward in the TD, accompanied by a range of reduced heatwaves eastward. As the dust concentration in the TD began to decrease gradually on July 9–10, the AOD also decreased, indicating the end of the dust storm. Meanwhile, the heatwave range remained only in the eastern TD.

The distribution of summer mean DMAT in the TD during 2000–2022 (Figure 5a) indicates that the summer DMAT in the TD is mainly over  $30^{\circ}C$ , with most of the region exceeding  $32.5^{\circ}C$  and a small region in the eastern portion at over  $35^{\circ}C$ . This suggests that the climate in the TD is ex-

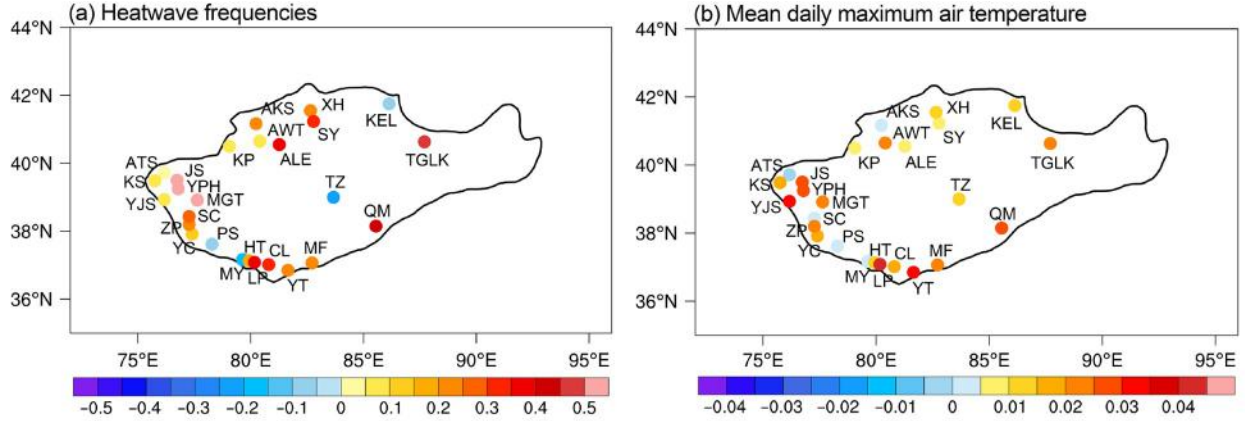


**Figure 2** Trend distribution of (a) heatwave frequencies (day year<sup>-1</sup>) and (b) DMAT (°C year<sup>-1</sup>) observed at each site in summer during 1993–2022. The region enclosed by the solid curve indicates the Tarim Basin where the TD is located.

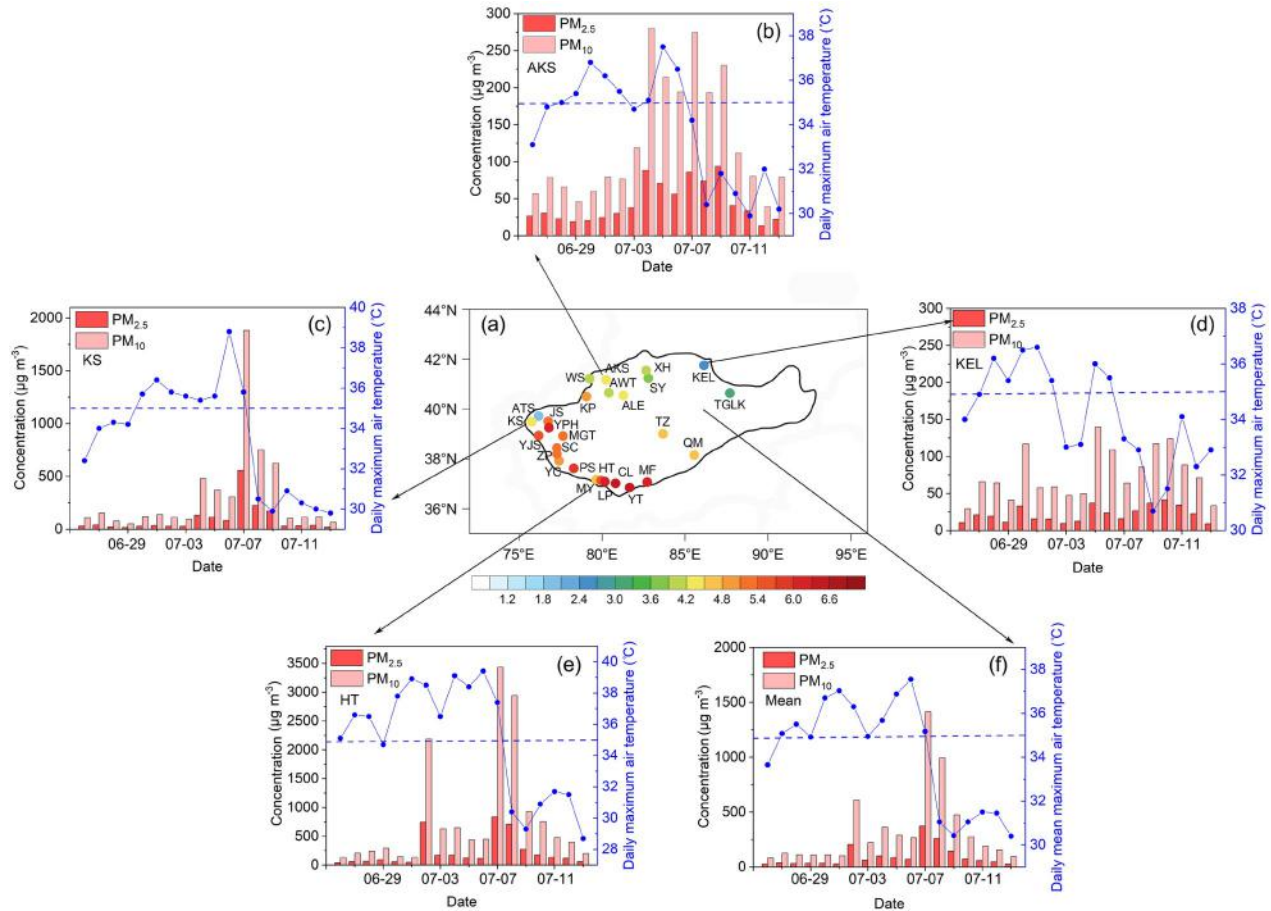


**Figure 3** Daily maximum air temperature (DMAT; °C), PM<sub>2.5</sub>, PM<sub>10</sub> concentrations ( $\mu\text{g m}^{-3}$ ) in a typical heatwave from June 25 to July 13, 2022, in the TD. (a) Spatial difference distribution of DMAT in the above heatwave relative to the mean DMAT in summer during 1993–2022. Variations of PM<sub>2.5</sub>, PM<sub>10</sub> concentrations and DMAT during the typical heatwave at (b) Akesu (AKS), (c) Kashi (KS), (d) Kerle (KEL), (e) Hetian (HT), and (f) average at all sites. The region enclosed by the solid curve in (a) indicates the Tarim Basin where the TD is located.

ceptionally hot in summer and highly conducive to extreme heatwaves in the case of a specific weather system. Meanwhile, as shown in Figure 5b, the summer-averaged AOD was over 0.4 in the central and southern TD and even reached up to 0.6 in the southern and southeastern TD. Analyzing the

anomalies of DMAT and AOD during the heatwave-dust period (from June 25 to July 13, 2022) relative to the summer averages during 2000–2022, we found that the anomalies of DMAT were mainly distributed in the central and western TD, with most anomalies exceeding 6°C. Simultaneously, the

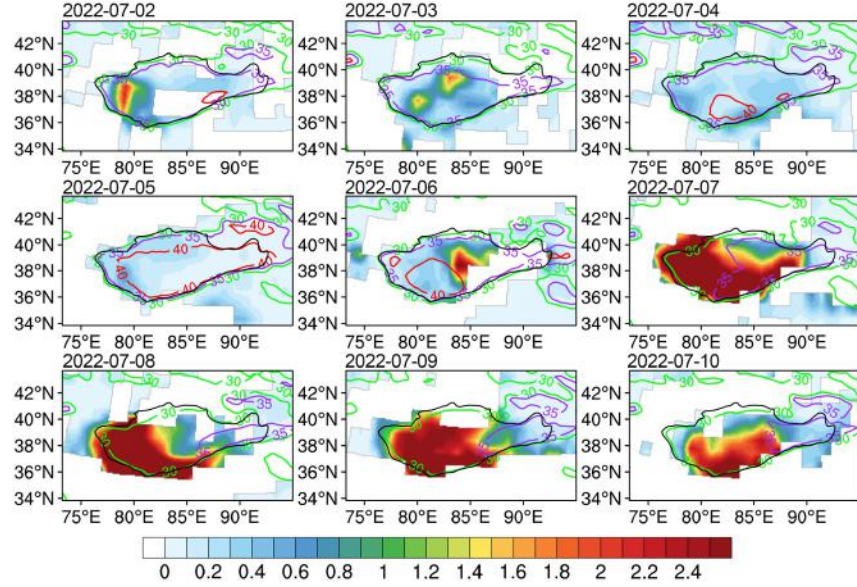


**Figure 4** Spatial distribution of air temperature (contours;  $^{\circ}\text{C}$ ) and AOD (colors) from July 2 to 10, 2022, during the heatwave period (from June 25 to July 13, 2022) in the TD. The region enclosed by the solid curve indicates the Tarim Basin where the TD is located. The green, purple, and red lines denote the isotherms of  $30^{\circ}\text{C}$ ,  $35^{\circ}\text{C}$ , and  $40^{\circ}\text{C}$ , respectively.

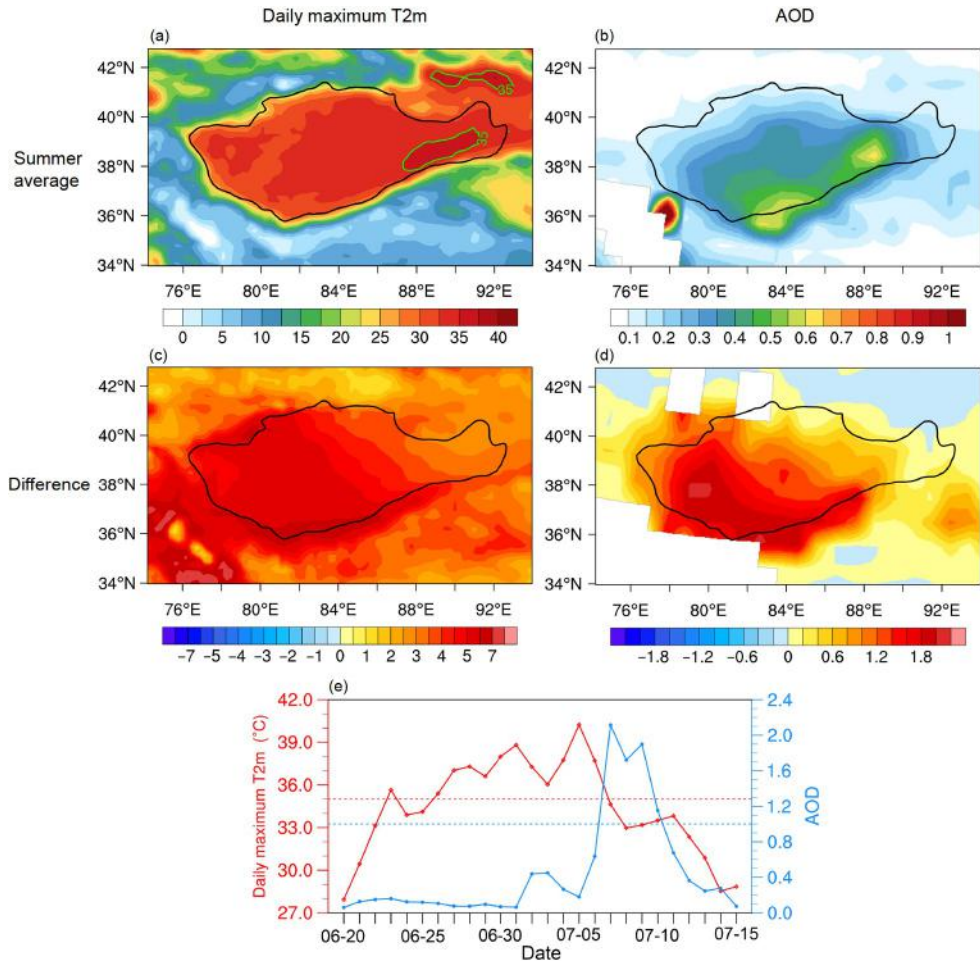


**Figure 5** Spatial distribution of summer mean (a) DMAT from ERA5 data ( $^{\circ}\text{C}$ ) and (b) AOD from MODIS data during 2000–2022 and the anomalies of (c) DMAT ( $^{\circ}\text{C}$ ) and (d) AOD during the heatwave-dust storm period (from June 25 to July 13, 2022) relative to the summer average during 2000–2022. (e) Time series of the regional average of DMAT and AOD during the heatwave-dust period in the Tarim Basin. The green line denotes the isotherms of  $35^{\circ}\text{C}$ . The region enclosed by the solid curve indicates the Tarim Basin where the TD is located.

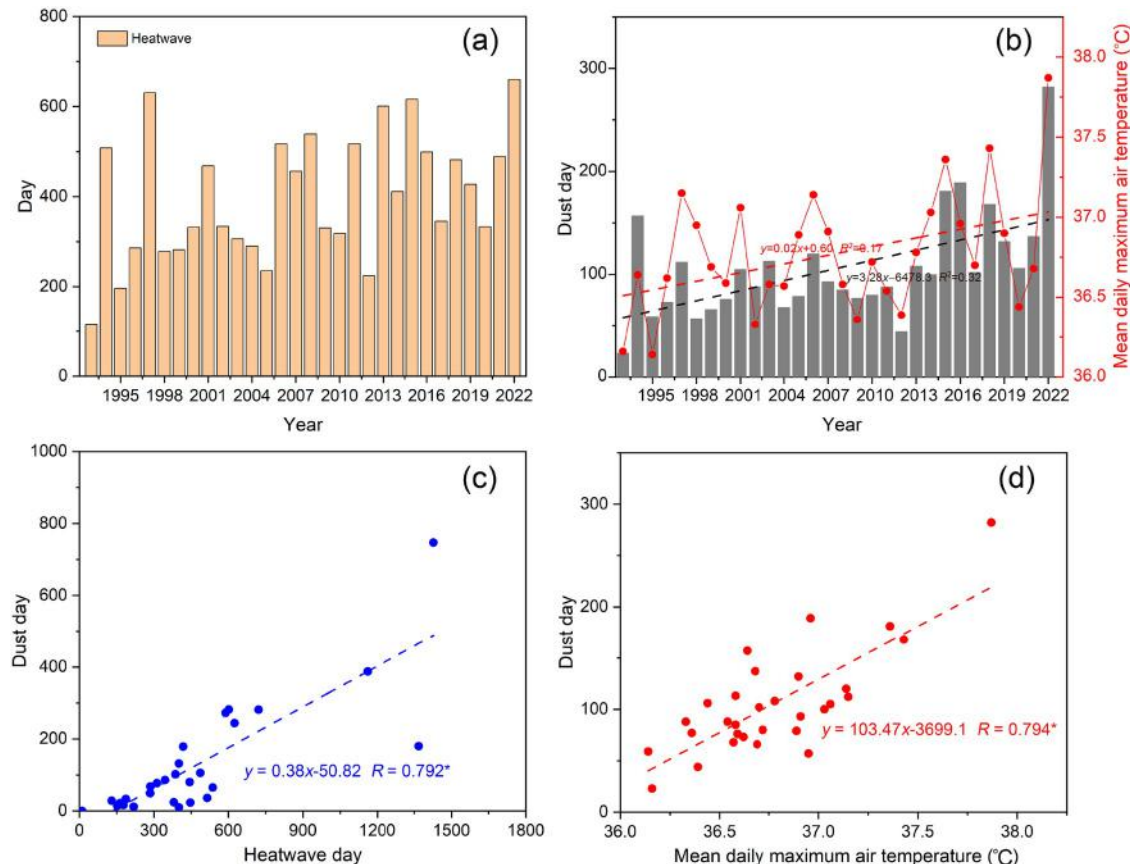
anomalies of AOD were mainly distributed in the southwestern TD, with anomalies generally over 1.2 and even over 1.8, which were two to three times the summer-averaged AOD. Notably, the anomalies of daily maximum temperature and AOD were distributed in the western and southern TD during the heatwave-dust event, implying a connection between the heatwave and the dust storm.

Figure 5e shows the time series of the regional averages of DMAT and AOD during the heatwave-dust period in the TD. The regional mean DMAT in the TD exceeded 35°C on June 26 and remained over 35°C in the following 10 days. In particular, a weak dust event occurred in the western and northern TD on July 2–3 (Figure 4), leading to a slight decrease in the regional-averaged DMAT in the TD. The regional averaged AOD in the TD started to increase on July 6 and quickly reached over 2.0 on July 7, accompanied by the decrease in the regional averaged DMAT lower than 35°C. In the following days, the DMAT continued to decrease in the TD because of the radiative effect of dust. Obviously, the occurrence of dust storms in the TD significantly lagged behind the heatwave, consistent with ground-based observations (Figure 3).

Furthermore, on the basis of the long-term observations of

the heatwaves and dust events in the TD over the past 30 years, a statistical analysis was performed. As shown in Figure 6a, the frequency of heatwaves showed an overall increasing tendency, especially significantly increasing since 2005. Over the past 30 years, the maximum frequency of heatwaves was 660 days, suggesting an average of about 24 heatwave days at each station. Meanwhile, the maximum frequency of dust events was 282 days, implying that 42.7% of the heatwave processes experienced dust events. Simultaneously, as shown in Figure 6b, the DMAT presented an increasing trend at a rate of 0.02°C per year over the past 30 years, consistent with Figure 2b. Furthermore, Figures 6c and 6d reveal significant positive correlations between dust frequency and heatwaves (including frequency and DMAT) after detrending. Overall, the more frequent and intense the heatwaves are, the more dust events occur.

Additionally, according to the first and third quartiles of the regional heatwave frequencies after detrending in the TD during 2000–2022, the high- and low-occurrence years of heatwaves were selected. The selected high-occurrence heatwave years include 2002, 2006, 2008, 2013, 2015 and 2016; and the low-occurrence years are 2000, 2003, 2005, 2012, 2020 and 2021.



**Figure 6** Association between dust events and heatwaves in the TD in summer during 1993–2022. (a) Frequency time series of heatwaves (day) and dust events (day) at the observational sites. (b) Time series of DMAT and dust event frequency (day). (c) Correlation between dust days and heatwave days after detrending. (d) Correlation between dust days and mean DMAT after detrending. The asterisks in (c) and (d) denote that correlation coefficients are significant above the 90% confidence level.

According to the selected high- and low-occurrence heatwave years, the distributions of AOD, soil temperature, and soil moisture of 0–10 cm underground in the summer of high- and low-occurrence heatwave years and their anomalies in the TD are shown in Figure 7. During the high-occurrence heatwave years, AOD values exceeding 0.4 are distributed across most of the TD, with the highest AOD values in the southeast of TD, followed by northeastern areas (Figure 7a). In contrast, during the low-occurrence heatwave years, AOD values exceeding 0.4 are only found in the southwestern TD (Figure 7d). The difference in AOD between the high- and low-occurrence heatwave years indicates that AOD is significantly higher in the high-occurrence heatwave years in the TD, especially in the central TD, with maximum anomalies up to 0.1 (Figure 7g). It reveals that dust events are more frequent and intense in high-occurrence heatwave years.

Besides, during the high-occurrence heatwave years, the soil temperature from 0 to 10 cm underground generally exceeded 30°C in most areas of the TD, even reaching over 32°C (Figure 7b). In contrast, during the low-occurrence heatwave years, the soil temperature from 0 to 10 cm underground rarely exceeded 30°C (Figure 7e). Obviously, the

difference in surface soil temperature was positive, especially in the central and northwestern TD (Figure 7h), corresponding to the positive anomalies of AOD. Meanwhile, the soil moisture from 0 to 10 cm underground in the high-occurrence heatwave years was lower (Figures 7c, 7f, 7i), especially in the west-central TD. This reveals that, in the high-occurrence heatwave years, higher soil temperatures and surface air temperatures induce drier soil in the TD, which is favorable for dust emission (Yang et al., 2019), resulting in more and stronger dust events.

### 3.3 Dynamic mechanism of compound events of heatwave and dust storm

Figure 8 shows the distributions of geopotential height fields at different layers, and the longitudinal cross-section of geopotential height anomalies averaged within 83°–90°E. In the high-occurrence heatwave years, the South Asian High (SAH) at 200 hPa was relatively weaker with a southern center, resulting in weaker westerlies (Figures 8a, 8b) and a strong anomalous anticyclone (anomalous high-pressure system) over the TD (Figure 8c). Meanwhile, a large-scale wave train of “cyclone-anticyclone-cyclone” was stimulated

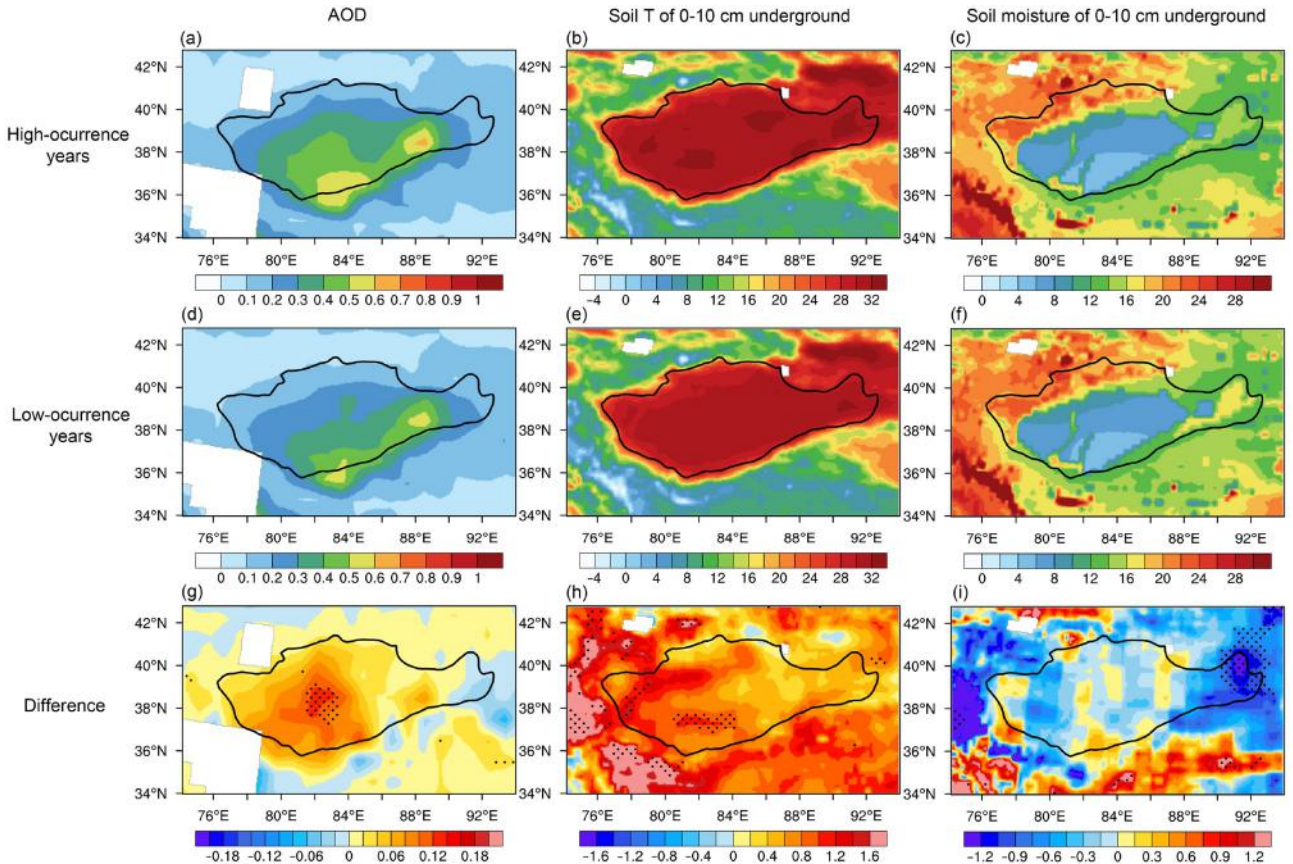


**Figure 7** Distributions of AOD derived from the MODIS product ((a), (d)), soil temperature ((b), (e), °C) and soil moisture 0–10 cm underground from GLDAS ((c), (f)  $\text{kg m}^{-2}$ ) in the summer of high- and low-occurrence heatwave years and differences of AOD (g), soil temperature (h), and soil moisture (i) between high- and low-occurrence heatwave years during 2000–2022. The region enclosed by the solid curve indicates the Tarim Basin where the TD is located. The black dots in (g), (h), and (i) indicate that anomalies are significant at the 90% confidence level.

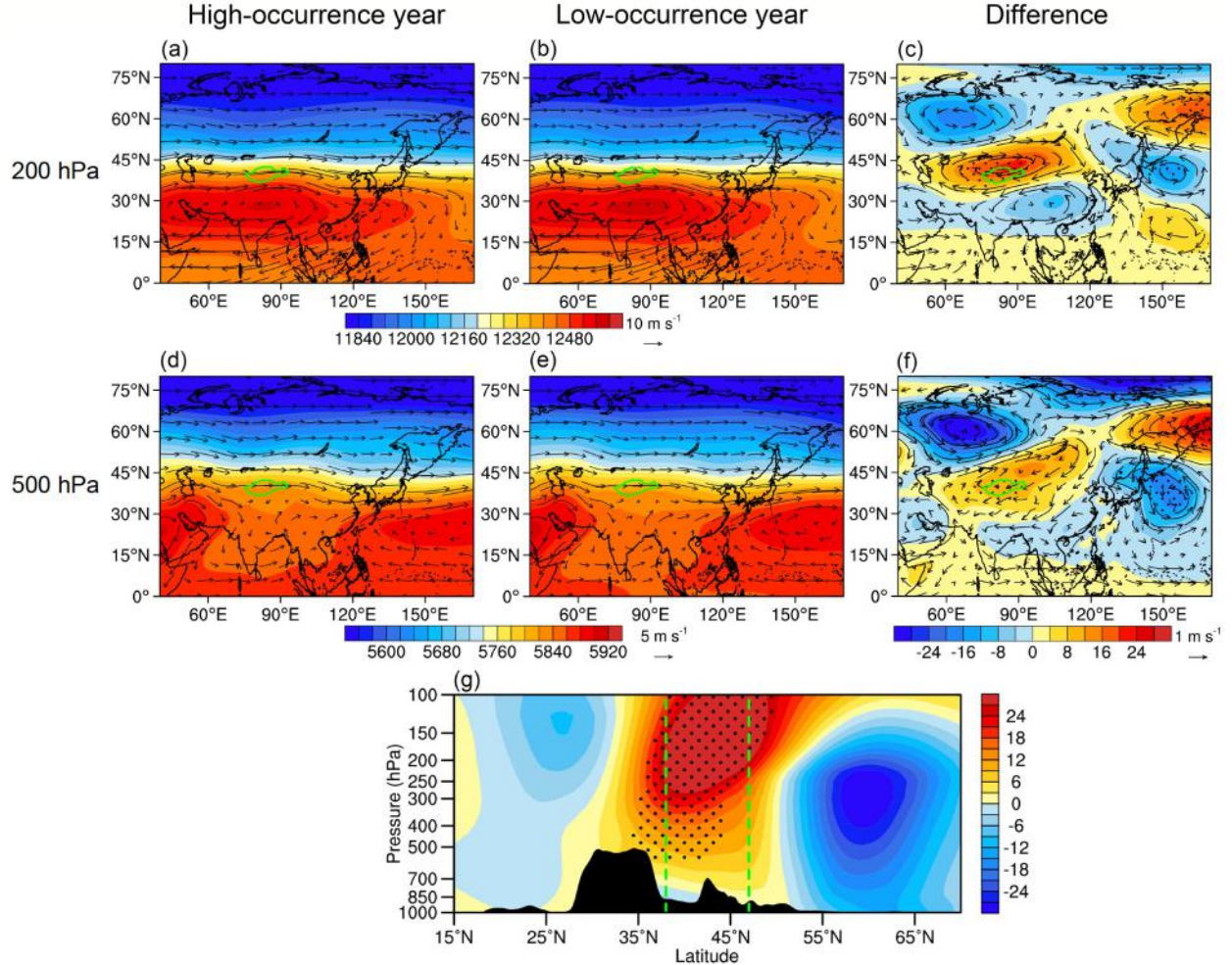


**Figure 8** Geopotential height fields (color shading; gpm) and horizontal wind fields (vector;  $\text{m s}^{-1}$ ) at 200 hPa ((a), (b)) and 500 hPa ((d), (e)) from ERA5 in the summer of high- and low-occurrence heatwave years and anomalies of geopotential height (color shading; gpm) and horizontal wind fields (vector;  $\text{m s}^{-1}$ ) ((c), (f)) between high- and low-occurrence years during 2000–2022. Panel (g) indicates the cross-section of anomalies in the geopotential height field averaged within  $83^{\circ}$ – $90^{\circ}$ E between high- and low-occurrence years. The region enclosed by the green curve in ((a)–(f)) indicates the Tarim Basin where the TD is located. The black shading in (g) denotes the topography. The dashed green line in (g) indicates the location of Tarim Basin. The black dots in (c), (f), and (g) denote significant anomalies at the 90% confidence level.

in the southeast-northwest direction at 200 hPa, favoring the maintenance of an anomalous anticyclone over the TD. At 500 hPa, the intensity of the West Pacific Subtropical High (WPSH) was weaker, and its position was more eastward in the high-occurrence heatwave years (Figures 8d, 8e), leading to a strong anomalous anticyclone (Figure 8f). The squeezing by two strong anomalous cyclones on both sides of the anomalous anticyclone was conducive to the maintenance of the anomalous anticyclone. From the cross-section of the anomalies in the geopotential height field averaged within  $83^{\circ}$ – $90^{\circ}$ E between the high- and low-occurrence heatwave years, the anomalous high pressure over the TD extended almost from the surface to over 100 hPa. Controlled by the strong high-pressure system, the TD experiences sunny and less cloudy conditions, which are favorable for the occurrence of heatwaves.

Furthermore, the vertical distributions of meteorological

element anomalies over the TD in heatwave anomalous years were analyzed. As shown in Figure 9a, in the high-occurrence heatwave years, the TD was controlled by descending motions, and the temperature was over  $24^{\circ}\text{C}$  below 850 hPa. According to the temperature difference between the high- and low-occurrence heatwave years (Figure 9b), positive air temperature anomalies from the surface to 250 hPa were found over the TD, with great anomalies up to  $0.9$ – $1.05^{\circ}\text{C}$ . Combined with positive geopotential height anomalies above 500 hPa (Figure 8g), a strong, warm, high-pressure system was found over the TD in the high-occurrence heatwave years, resulting in descending motions (Figure 9c). Moreover, Figure 9d shows negative specific humidity anomalies from the surface to 500 hPa over the TD in the high-occurrence heatwave years, especially with anomalies up to  $-0.18 \text{ g kg}^{-1}$  in the southern TD, implying less precipitation and maintained heatwaves. Meanwhile, less precipitation

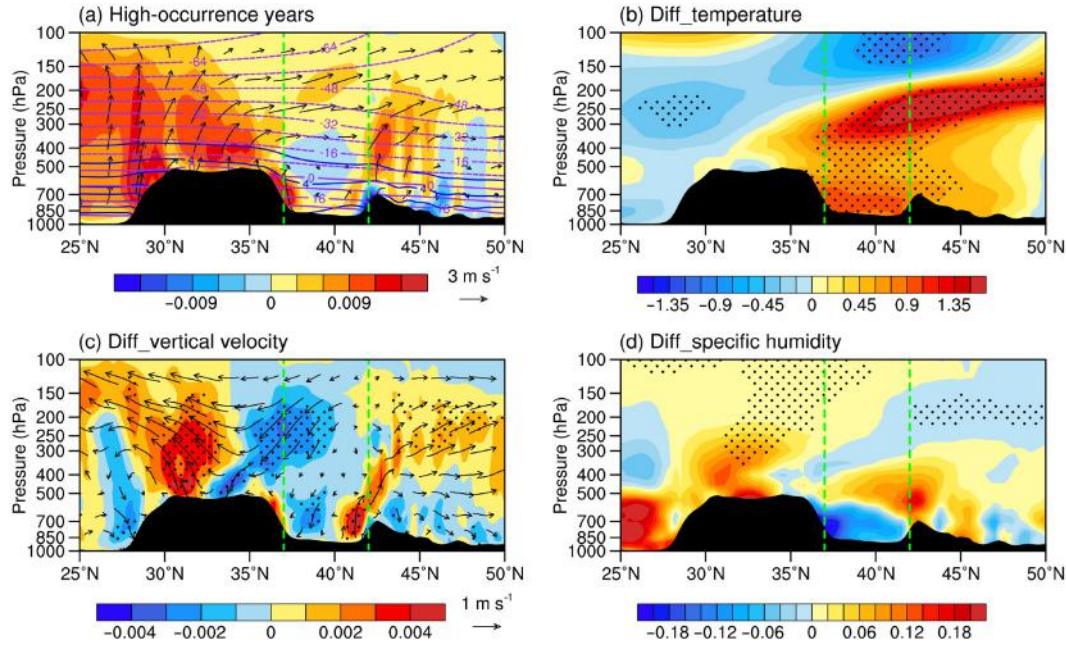


**Figure 9** Cross-sections of the temperature (purple contours;  $^{\circ}\text{C}$ ), vertical velocity (color shading;  $\text{m s}^{-1}$ , with positive values indicating ascending motions), wind field (vectors of  $u$  and  $w^*300$ ;  $\text{m s}^{-1}$ ), and specific humidity (blue contours;  $\text{g kg}^{-1}$ ) averaged within  $80^{\circ}\text{--}85^{\circ}\text{E}$  from ERA5 in the summer of high-occurrence heatwave years in the TD (a) and differences between the high- and low-occurrence heatwave years ((b)–(d)). The black shading indicates topography. The dashed green lines indicate the location of the Tarim Basin where the TD is located. The black dots in (b), (c), and (d) denote significant anomalies at the 90% confidence level.

caused lower soil moisture in the TD, which was favorable for dust emissions.

#### 4. Conclusions and discussions

In this study, we analyzed the characteristics of heatwaves and dust events and their relationship in the TD during 1993–2022. Also, a dynamic mechanism of compound events of heatwave and dust storm was proposed. The main conclusions are as follows:

In the past 30 years, the frequency and intensity of heatwaves showed increasing trends in the TD, with mean growth rates of  $0.21 \text{ days year}^{-1}$  and  $0.02^{\circ}\text{C year}^{-1}$ , respectively. Furthermore, heatwaves with DMAT exceeding  $40^{\circ}\text{C}$  showed an increasing trend in recent years. We found that the frequency and intensity of heatwaves were positively correlated with dust events, with a maximum of over 40% of heatwaves existed with dust events.

According to the first and third quartiles of the regional-averaged heatwave frequencies in the TD after detrending for 2000–2022, we found that the AOD showed positive anomalies in the high-occurrence heatwave years in the TD, especially in the central TD. Besides, during the high-occurrence heatwave years in the TD, higher air temperatures were accompanied by lower soil moisture and higher soil temperatures, which favored dust emissions in the TD. In the high-occurrence heatwave years, the SAH at 200 hPa was

weaker with a southern center, inducing weaker westerlies over the TD. Simultaneously, in high-occurrence heatwave years, the WPSH was weaker at 500 hPa, leading to strong anomalous anticyclones over the TD. Meanwhile, a large-scale wave train of “cyclone-anticyclone-cyclone” was stimulated in the southeast-northwest direction, promoting sunny and less cloudy weather in the TD and thus leading to stronger and longer heatwaves. Consequently, low specific humidity and less precipitation led to lower soil moisture, which was conducive to dust emissions, thus leading to more and stronger dust events.

This study provides a basis for understanding compound extreme events of heatwave and dust event in the Tarim Basin where the TD is located, as well as some clues for forecasting heatwave-dust storms.

**Acknowledgements** This work was supported by the National Natural Science Foundation of China (Grant Nos. 41991231 and 91937302) and the Fundamental Research Funds for the Central Universities (Grant No. lzujbky-2022-kb11).

**Conflict of interest** The authors declare that there are no conflicts of interest.

#### References

- Aryal Y N, Evans S. 2021. Global dust variability explained by drought sensitivity in CMIP6 models. *J Geophys Res-Earth Surf*, 126: e2021JF006073
- Bai W, Gu X, Li S, Tang Y, He Y, Gu X, Bai X. 2018. The performance of

multiple model-simulated soil moisture datasets relative to ECV satellite data in China. *Water*, 10: 1384

Bastos A, Gouveia C M, Trigo R M, Running S W. 2014. Analysing the spatio-temporal impacts of the 2003 and 2010 extreme heatwaves on plant productivity in Europe. *Biogeosciences*, 11: 3421–3435

Chen S Y, Wang J S, Guo J T, Lu X D. 2012. Evolution characteristics of the extreme high temperature event in Northwest China from 1961 to 2009 (in Chinese). *J Nat Resour*, 27: 832–844

Ding T, Qian W, Yan Z. 2010. Changes in hot days and heat waves in China during 1961–2007. *Intl J Clim*, 30: 1452–1462

Feng S, Hao Z, Zhang X, Hao F. 2019. Probabilistic evaluation of the impact of compound dry-hot events on global maize yields. *Sci Total Environ*, 689: 1228–1234

IPCC. 2013. Climate Change 2013: The Physical Science Basis. In: Stocker T F, Qin D, Plattner G K, Tignor M, Allen S K, Boschung J, Nauels A, Xia Y, Bex V, Midgley P M, eds. Contribution of Working Group I to the Fifth Assessment Report of the Intergovernmental Panel on Climate Change. Cambridge: Cambridge University Press. 1535

IPCC. 2021. Climate Change 2021: The Physical Science Basis. In: Masson-Delmotte V, Zhai P, Pirani A, Connors S L, Péan C, Berger S, Caud N, Chen Y, Goldfarb L, Gomis M I, Huang M, Leitzell K, Lonnoy E, Matthews J B R, Maycock T K, Waterfield T, Yelekçi O, Yu R, Zhou B, eds. Contribution of Working Group I to the Sixth Assessment Report of the Intergovernmental Panel on Climate Change. Cambridge: Cambridge University Press. 2391

Hersbach H, Bell B, Berrisford P, Hirahara S, Horányi A, Muñoz-Sabater J, Nicolas J, Peubey C, Radu R, Schepers D, Simmons A, Soci C, Abdalla S, Abellan X, Balsamo G, Bechtold P, Biavati G, Bidlot J, Bonavita M, De Chiara G, Dahlgren P, Dee D, Diamantakis M, Dragani R, Flemming J, Forbes R, Fuentes M, Geer A, Haimberger L, Healy S, Hogan R J, Hölm E, Janisková M, Keeley S, Laloyaux P, Lopez P, Lupu C, Radnoti G, de Rosnay P, Rozum I, Vamborg F, Villaume S, Thépaut J. 2020. The ERA5 global reanalysis. *Quart J R Meteorol Soc*, 146: 1999–2049

Jin R, Wu Z, Zhang P. 2018. Tibetan Plateau capacitor effect during the summer preceding ENSO: from the Yellow River climate perspective. *Clim Dyn*, 51: 57–71

Kaufman Y, Tanré D, Remer L, Vermote E, Chu A, Holben B. 1997. Operational remote sensing of tropospheric aerosol over land from EOS moderate resolution imaging spectroradiometer. *J Geophys Res-Atmos*, 102: 17051–17067

Li B, Chen Y, Shi X, Chen Z, Li W. 2013. Temperature and precipitation changes in different environments in the arid region of northwest China. *Theor Appl Climatol*, 112: 589–596

Lyamani H, Olmo F J, Alcántara A, Alados-Arboledas L. 2006. Atmospheric aerosols during the 2003 heat wave in southeastern Spain I: Spectral optical depth. *Atmos Environ*, 40: 6453–6464

Pu B, Jin Q, Ginoux P, Yu Y. 2022. Compound heat wave, drought, and dust events in California. *J Clim*, 35: 8133–8152

Qian Z A, Wu T W, Song M H, Ma X B, Cai Y, Liang X Y. 2001. Arid disaster and advances in arid climate researches over Northwest China (in Chinese). *Adv Earth Sci*, 16: 28–38

Robine J M, Cheung S L K, Le Roy S, Van Oyen H, Griffiths C, Michel J P, Herrmann F R. 2008. Death toll exceeded 70,000 in Europe during the summer of 2003. *Compt Rendus Biolog*, 331: 171–178

Rodell M, Houser P R, Jambor U, Gottschalck J, Mitchell K, Meng C J, Arsenault K, Cosgrove B, Radakovich J, Bosilovich M, Entin J K, Walker J P, Lohmann D, Toll D. 2004. The global land data assimilation system. *Bull Amer Meteorol Soc*, 85: 381–394

Sayer A M, Hsu N C, Bettenhausen C, Jeong M. 2013. Validation and uncertainty estimates for MODIS Collection 6 “Deep Blue” aerosol data. *J Geophys Res-Atmos*, 118: 7864–7872

Smoyer-Tomic K E, Kuhn R, Hudson A. 2003. Heat wave hazards: An overview of heat wave impacts in Canada. *Nat Hazards*, 28: 465–486

Wang J, Niu S J, Shen J G. 2009. Spatiotemporal distribution of sand-dust storm in xilingol league and its correlation with climate factors (in Chinese). *J Natur Disast*, 18: 209–216

Wang C, Li Z, Chen Y, Ouyang L, Li Y, Sun F, Liu Y, Zhu J. 2023. Drought-heatwave compound events are stronger in drylands. *Weather Clim Extremes*, 42: 100632

Wang S, Wang J, Zhou Z, Shang K. 2005. Regional characteristics of three kinds of dust storm events in China. *Atmos Environ*, 39: 509–520

Wu H, Su X, Singh V P. 2021. Blended dry and hot events index for monitoring dry-hot events over global land areas. *Geophys Res Lett*, 48: e2021GL096181

Wu Z, Yu L. 2016. Seasonal prediction of the East Asian summer monsoon with a partial-least square model. *Clim Dyn*, 46: 3067–3078

Yang K, Zhang J. 2018. Evaluation of reanalysis datasets against observational soil temperature data over China. *Clim Dyn*, 50: 317–337

Yang X, Zhou C, Huo W, Yang F, Liu X, Mamtimin A. 2019. A study on the effects of soil moisture, air humidity, and air temperature on wind speed threshold for dust emissions in the Taklimakan Desert. *Nat Hazards*, 97: 1069–1081

Yuan X, Wang L, Wu P, Ji P, Sheffield J, Zhang M. 2019. Anthropogenic shift towards higher risk of flash drought over China. *Nat Commun*, 10: 4661

Zhou C, Liu Y, Zhu Q, He Q, Zhao T, Yang F, Huo W, Yang X, Mamtimin A. 2022a. *In situ* observation of warm atmospheric layer and the heat contribution of suspended dust over the Tarim Basin. *Atmos Chem Phys*, 22: 5195–5207

Zhou C, Liu Y, He Q, Zhong X, Zhu Q, Yang F, Huo W, Mamtimin A, Yang X, Wang Y, Meng L. 2022b. Dust characteristics observed by unmanned aerial vehicle over the Taklimakan Desert. *Remote Sens*, 14: 990

Zhou C, Mamtimin A, Pan H, Yang F, Huo W, Meng L, Jin L, Yang X. 2019. Relationship between air temperature and horizontal sand-dust flux observed in the Taklimakan Desert, China. *Theor Appl Climatol*, 138: 1845–1852

Zou X, Zhai P, Zhang Q. 2005. Variations in droughts over China: 1951–2003. *Geophys Res Lett*, 32: 2004GL021853